ACS APPLIED MATERIALS & INTERFACES

RESEARCH ARTICLE

www.acsami.org

Cross-Linked Perylene Diimide-Based n-Type Interfacial Layer for Inverted Organic Photovoltaic Devices

Alexander W. Hains,* Hsiang-Yu Chen, Thomas H. Reilly, III, and Brian A. Gregg*

National Renewable Energy Laboratory, 1617 Cole Boulevard, Golden, Colorado 80401, United States

ABSTRACT: This contribution describes the synthesis and characterization of a perylene diimide (PDI)-based n-type semiconductor and its application to organic photovoltaic (OPV) devices having inverted architecture. Films of *N*,*N*′-bis(3-trimethoxysilylpropyl)-1,6,7,12-tetrachloroperylene-3,4,9,10-tetracarboxyldiimide (Cl_4PSi_2) and blends of this material with various polymers are solution-deposited on tin-doped indium oxide (ITO) substrates as interfacial layers (IFLs). The organic IFL described in this work is based on the air- and light-stable PDI core, annealed at low temperatures compatible with flexible substrates, and crosslinks in air for compatibility with device fabrication. Morphological, optical, and electrochemical analysis of these IFL films demonstrate predominantly smooth surfaces and HOMO and LUMO energies of ∼4.5 and 7.0 eV, respectively, which are ideal for accepting electrons and blocking holes in inverted devices. A cationic silane species is added to the Cl_4PSi_2 at an optimum ∼2−5 wt % to reduce IFL series resistance and enhance device performance. Also, a short light soaking procedure is necessary for completed devices to achieve high fill factors in current density−voltage analysis, a phenomenon previously only observed for inverted devices having an n-type inorganic IFL.

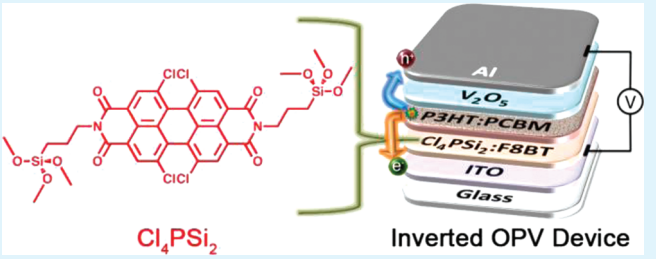

KEYWORDS: organic photovoltaics, solar cells, organic electronics, interfacial layer, inverted architecture

1. INTRODUCTION

Organic photovoltaics (OPVs) possess significant potential advantages over their inorganic counterparts, such as inexpensive fabrication and flexible substrate compatibility, and they have therefore garnered great attention and a focused research effort in recent years[1−10] with certified efficiencies of 7−8% now reported in the literature.[11,12] Many individual building blocks and processes of OPV devices require simultaneous optimization and harmonious interaction to achieve high overall power conversion efficiency (η_P). Among these components, interfacial layers (IFLs) represent a vital OPV device element, although the literature focus on them has been less than on other aspects of OPVs, such as novel active layer materials. Intelligent interface design is essential in promoting beneficial coordination between the various layers in multilayered optoelectronic devices such as OPVs, and the large, direct influence of IFLs over OPV device performance is unmistakable.[13−15] But how exactly does an interface modify device operation, and what aspects of IFL design need consideration in order to impart beneficial properties to device function?

Devices without interfacial layers (IFLs) tend to exhibit inferior performance compared to devices that incorporate an appropriate additional layer or layers into their design. In general, IFLs serve a variety of important functions in a device, and many considerations must be addressed for their optimal design and employment.[13−17] First, IFLs work to transport charges of just one type, either holes or electrons, from the active layer to the electrode, while simultaneously acting as a barrier to passage of charges of the other type. Such a selective contact is important to properly rectify the current and prevent deleterious charge recombination at the electrode. This is achieved in part by examining the frontier energy levels of the IFL material and aligning them properly with the active layer donor (D) and acceptor (A) energies such that charge transfer in the desired direction is favorable, and a large energetic barrier is present for the transfer of the undesired charge species. Additional IFL influence is observed in the nature of the contacts to both the electrode and active layer. In OPVs, an IFL on tin-doped indium oxide (ITO) needs to fulfill the challenging role of making intimate contact to a hydrophilic inorganic surface while also maintaining good adhesion to the covering organic active layer, which is often hydrophobic. The density of charge transfer sites at these interfaces and their stability over time and towards various external conditions such as heat, light, and humidity, all strongly affect OPV performance.[16,18−22] Another consideration in IFL design is that the layer, if placed on the light-incident side of the device, does not interfere with the active layer light absorption responsible for current generation. This implies that the IFL is required to be either very thin or else optically transparent in the region of active layer absorption. If the IFL is instead inserted before the reflective back electrode, then its influence on the optical interference pattern of the incident and

Received: August 2, 2011
Accepted: October 21, 2011
Published: November 07, 2011

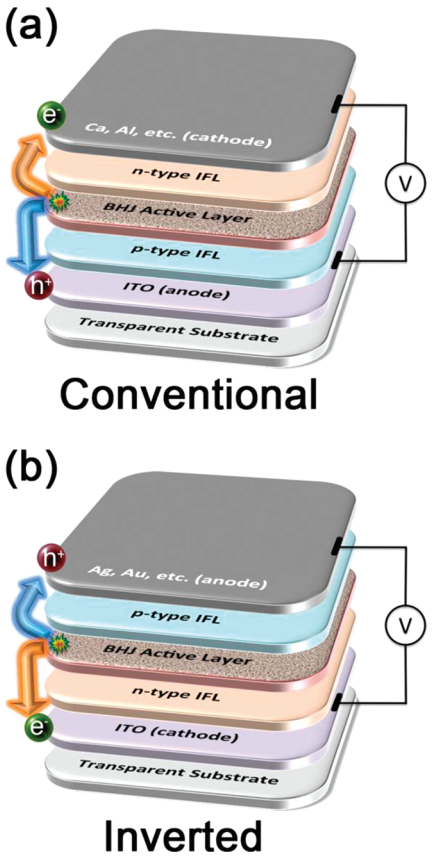

Figure 1. (a) Conventional and (b) inverted device architectures are illustrated.

reflected light should be considered and the IFL thickness adjusted to properly align the positive interference with the active layer to maximize the potential light absorption and short-circuit current density (J_{sc}) of the device.[1,23,24]

To date, most work that focuses on OPV IFLs strives to devise a suitable p-type film that constitutes a replacement for the ubiquitous, but oft derided, PEDOT:PSS.[16,17,25−30] This is likely because conventional device architecture (Figure 1a) defines that holes are collected at the ITO interface, and therefore any IFL deposited on ITO in a conventional device should be p-type to allow for facile charge extraction. Inverted devices, as the name implies, collect electrons at the ITO electrode and require an ITO-side IFL to be n-type. Devices of inverted architecture (Figure 1b) possess several advantages over their more common conventional counterparts. First, they completely avoid the problematic ITO/PEDOT:PSS interface, which has been shown to be unstable and lead to device failure.[16,31−33] Second, the inverted geometry allows the use of air-stable, high-work-function metal electrodes, such as gold or silver.[34,35] These metals are amenable to printing, thereby eliminating a relatively expensive high vacuum deposition process.[36−38] The use of silver as an electrode material has also been shown to produce an increase in efficiency with prolonged air exposure since the native oxide layer that builds up on Ag increases its work function and benefits inverted OPV performance.[39] Another key advantage of the inverted design stems from the active layer morphology. It has recently been shown that the vertical phase separation in many common OPV materials systems, including poly(3-hexylthiophene) (P3HT):[6,6]-phenyl-C_{61}-butyric acid methyl ester (PCBM) bulk heterojunctions (BHJ), yields a film with a high density of PCBM at the substrate interface and enriched P3HT concentration near the air interface as spin-coated.[40] This vertical film morphology represents an inherent advantage of the inverted architecture in which the electron and hole transporting materials are properly congregated near the ITO and metal electrodes, respectively, for efficient charge extraction in the inverted direction.[13,36,40−43] Finally, ITO itself is an n-type transparent conducting oxide (TCO) and therefore is easily able to fulfill the role of collecting electrons. Its work function of ∼4.5−4.7 eV is approximately intermediate between the HOMO and LUMO energies of commonly used organic donors and acceptors, which means that depending on its surface modification it can be well-suited for either hole or electron collection.[42]

Although PEDOT:PSS clearly represents the most commonly used literature p-type IFL to coat ITO for hole collection, comparatively few n-type IFL materials have been presented for electron collection. Of the compounds utilized to date, no obvious material choice exists for this role, and almost none of those used in devices are organic.[13,14,42] Some of the materials employed for this role are TiO_x,[44,45] ZnO,[34,46−49] Cs_2CO_3,[50,51] and at least one recent example of a self-assembled organometallic compound.[36] Most of these require a high-temperature sintering/annealing step that increases the cost of the device and is incompatible with plastic substrates. In a conscious effort to omit these high sintering temperatures while still selecting a material that exhibits excellent chemical stability in air and light, a perylene diimide (PDI) derivative was chosen for use as an IFL. In this work, a stable, organic, cross-linkable, perylene-based, n-type interfacial layer (IFL) is designed, characterized, and implemented into OPV devices having inverted architecture. The effects on OPV device metrics of blending this layer with an appropriate n-type semiconducting polymer and incorporating a cationic additive are also examined.

2. EXPERIMENTAL SECTION

Materials and Methods. All chemicals were used as received unless otherwise noted. Anhydrous chlorobenzene, anhydrous methanol, (3-aminopropyl)trimethoxysilane (APMS), *N*-trimethoxysilylpropyl-*N*,*N*,*N*-trimethylammonium chloride ($APMS^+$) (50% in methanol), and 99.9% acetonitrile were purchased from Aldrich, Cl_4PTCDA was purchased from AK Scientific Inc., poly(9,9′-dioctylfluorene-*co*-benzothiadiazole) (F8BT) was purchased from American Dye Source, Inc., P3HT (Plexcore OS 2100) was purchased from Plextronics, Inc., and PCBM was purchased from Nano-C, Inc. Tetrabutylammonium hexafluorophosphate ($Bu_4N^+PF_6^-$) was recrystallized twice from ethanol before use as a supporting electrolyte in electrochemical experiments. Optical absorption spectra were obtained with an Agilent 8453 UV-vis spectrophotometer. Film thicknesses were measured using a Dektak 8 Stylus Profiler. Cyclic voltammetery (CV) measurements were performed using scan rates of 10−100 mV/s with either ITO, Pt, or glassy carbon working electrodes in acetonitrile with 0.1 M $Bu_4N^+PF_6^-$ as the electrolyte. A platinum counter electrode and a Ag/AgCl reference electrode were employed, the Fc/Fc^+ couple was used to verify the validity of results, and the results were converted to the standard calomel electrode (SCE) scale using $E^0_{Ag/AgCl} = -0.045$ V vs SCE.[52] The measured reduction potentials were converted to the vacuum scale to determine the LUMO energies, or electron affinities (EA), using the following relationships (the first from ref 52, the second from refs 52 and 53)

$$E^{onset}_{red\ vs\ SCE} + 0.24V = E^{onset}_{red\ vs\ NHE}$$

$$4.5V - E^{onset}_{red\ vs\ NHE} = E_{LUMO}(eV)$$

Tapping mode AFM experiments were conducted using a Veeco Dimension 3100 with a Nanoscope V controller. Olympus cantilever tips made of Si with a tip radius of 9 nm were employed. OPV devices were evaluated with current density−voltage ($J-V$) scans taken in a N_2-filled glove box in the dark and under illumination. A home-built solar simulator previously described[19] was employed to analyze device $J-V$ response under 100 mW/cm^2 illumination from a tungsten halogen bulb monitored by two Si photodiodes.

Synthesis of *N,N′*-Bis(3-trimethoxysilylpropyl)-1,6,7,12-tetrachloroperylene-3,4,9,10-tetracarboxyldiimide (Cl_4PSi_2). A 0.29 M solution of APMS was made by diluting 0.50 mL of the Aldrich product to 10.0 mL with anhydrous CH_3OH. A two-neck round-bottom flask with a reflux condenser and filled with N_2 and evacuated on a Schlenk line three times before filling with 100.0 mg (1.886×10^{-4} mol) 1,6,7,12-tetrachloroperylene-3,4,9,10-tetracarboxylic acid (Cl_4PTCDA), 4.0 mL anhydrous CH_3OH, and 48.2 mL anhydrous chlorobenzene (CB). To this slurry, 1.4 mL of the APMS solution was added with stirring at room temperature, and then the reaction mixture was heated to 80 °C. The reaction became a clear, orange solution within about 1 min. The resulting solution is a 3.5 mM (3 mg/mL) solution of Cl_4PSi_2. The reaction progress was followed with thin-layer chromatography (TLC) on silica plates (CH_3OH:CB, 1:1), which shows the presence of an immobile spot, corresponding to the silanated product, appear while the mobile spot for Cl_4PTCDA disappears over ~8 h, and the reaction was cooled to room temperature after ~24 h. The silanated product proved difficult to characterize due to silanization of the NMR tube and the presence of small quantities of dimers and oligomers from crosslinking in solution. Although the expected NMR peaks were present, some of these impurities were also apparent. Therefore, to demonstrate the synthesis with a compound more amenable to characterization, the non-silanated analogue *N,N′*-bis(*n*-propyl)-1,6,7,12-tetrachloroperylene-3,4,9,10-tetracarboxyldiimide was prepared exactly as described above, and the product was characterized and readily apparent via NMR. For this compound, ^{1}H NMR (400 MHz, $CDCl_3$, 25 °C): δ 8.69 (s, 4H), 4.17 (t, J = 7.4 Hz, 4H), 1.73 (m, 4H), 1.03 (t, J = 7.4 Hz, 6H).

Cl_4PSi_2 Film Deposition. ITO-coated glass substrates are cleaned via successive 30-min ultrasonication treatments in soapy water, water (5 min), acetone, and 2-propanol, respectively, before being blown dry. The solvent-cleaned substrates are further cleaned with a 5 min UV ozone treatment immediately before layer deposition. A 3 mg/mL solution of Cl_4PSi_2 in CB:MeOH (9:1), containing the appropriate amount of "dopant" APMS$^+$ if necessary, is placed in a small petri dish, and a clean ITO substrate is immersed in this solution for 3 min, after which time it is removed and blown dry. The back of the substrate is immediately cleaned with a cotton swab dampened with CB:MeOH, and the substrate is annealed at 120 °C on a hot plate in air for 30 min to complete the crosslinking and render the IFL film insoluble. The film is then immersed into a solution of CB:MeOH (1:1) for 1 min and swirled to remove any insoluble material and blown dry.

OPV Device Fabrication. For inverted devices films of Cl_4PSi_2 were deposited as described above. A solution of P3HT:PCBM (1:0.8 by wt) in ODCB (20 mg/mL P3HT) was stirred overnight in the dark at 60 °C in a glove box. This solution was deposited by spin-coating at 550 rpm for 1 min, followed by 1500 rpm for 1 s to spin off excess solution. The wet films were placed in individual petri dishes to dry slowly. Once dry, the films were annealed at 110 °C for 10 min on a hot plate in a glove box. Finally, these substrates were transferred to a vacuum evaporator where V_2O_5 (10 nm, 0.2 Å/s) and Al (100 nm, ~20 Å/s) were sequentially evaporated at a pressure of 5×10^{-6} Torr or higher vacuum without breaking vacuum to complete the devices. The fast Al deposition from a W basket was beneficial in minimizing organic contamination from the walls of an evaporator mainly used to deposit organic small molecules. All devices were left unencapsulated and transferred immediately to a glove box for testing.

Scheme 1. Synthesis of Cl_4PSi_2

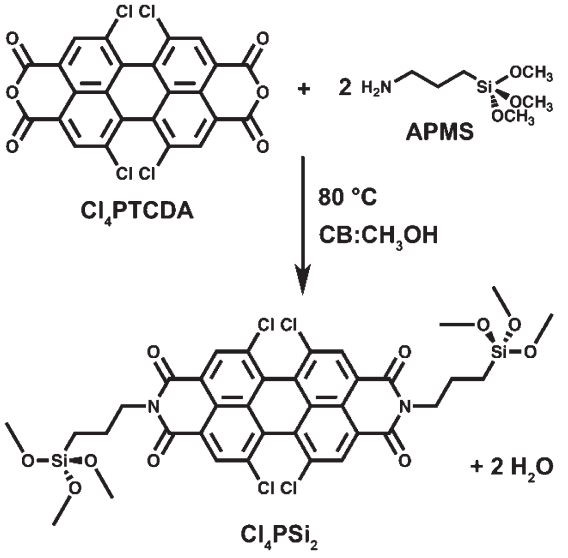

3. RESULTS AND DISCUSSION

Cl_4PSi_2 Synthesis. The synthesis of Cl_4PSi_2 portrayed in Scheme 1 and described in detail in the Experimental Section is a straightforward condensation of APMS with Cl_4PTCDA at 80 °C with stirring. The reaction product cannot be purified easily because the silane moieties are very reactive, so the one-step reaction solution is used to cast films without further purification. However, the presence of small quantities of either starting material is not expected to adversely affect film properties. The slight (< 5%) excess of APMS will actually aid crosslinking if it is not removed when the film is rinsed, and any remaining unreacted Cl_4PTCDA will be held in place by the crosslinked matrix of Cl_4PSi_2. As will be shown below, even rinsing the film does not cause any significant change in absorption, and this indicates that little if any non-cross-linked perylene derivative is present in films. Additionally, the electronic properties of the resulting films will remain unaffected by unreacted Cl_4PTCDA since the aromatic molecular core is essentially identical to that of the product.

The solvent selected for this reaction is an important consideration in the stability of the Cl_4PSi_2 solution and its propensity to crosslink. Initially, the synthesis was performed in pure chlorobenzene (CB), but the water produced as a by-product of the reaction induced formation of a crosslinked polymer that precipitated out of solution almost immediately. CH_3OH was added to deactivate the water generated and prevent spontaneous cross-linking. A balance in the CB:CH_3OH ratio was optimized experimentally at 9:1 to allow intentional crosslinking to proceed in air on a substrate surface but to stymie spontaneous crosslinking in solution such that a 3.5×10^{-3} M Cl_4PSi_2 solution stored under N_2 on a Schlenk line can be reliably used for several weeks.

Cl_4PSi_2 Film Characterization. Characterization of thin films of Cl_4PSi_2 was carried out via profilometry, AFM, optical absorption, and cyclic voltammetry to investigate film thickness, morphology, and optoelectronic properties.

Cl_4PSi_2 Surface Morphology. Initially, Cl_4PSi_2 films were formed by spin-coating from a solution of chlorobenzene and

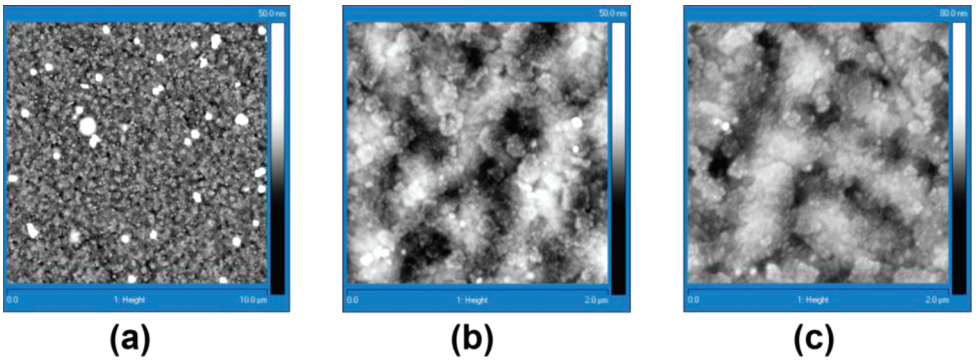

Figure 2. AFM images of films of (a) Cl_4PSi_2 made by spin-coating; (b) Cl_4PSi_2 formed from substrate immersion into a 1.2×10^{-3} M solution of Cl_4PSi_2 in CB:CH_3OH (9:1); (c) Cl_4PSi_2:F8BT (1:1 by wt) deposited by substrate immersion into an identical solution to part b, but with F8BT added. RMS roughnesses for parts a, b, and c are 12.4, 3.53, and 4.05 nm, respectively.

methanol. The resultant films exhibit low apparent crosslinking density (see below) and a rough surface morphology (rms roughness = 12.4 nm) that contain spikes of PDI over 100 nm in height (Figure 2a). Therefore another film deposition method was devised in which ITO substrates are immersed in a petri dish containing Cl_4PSi_2 dissolved in CB and methanol. AFM on the resultant films reveals far smoother (rms roughness = 3.53 nm) surfaces lacking the spikes that plagued the spin-cast films. Figure 2b depicts an AFM image of a Cl_4PSi_2 film formed by this immersion technique. Although the spikes are not present, there is some visible texture to the film through which the subgrains of the underlying ITO substrate appear in a few places. This indicates that despite forming a nearly conformal film with relative smoothness almost identical to the ITO, small regions of incomplete coverage exist, which could cause the corresponding sections of a completed solar cell to perform as though insufficient IFL material is present, negating the full advantage of the IFL in the device. A further step to mitigate this effect was made by blending the Cl_4PSi_2 with a polymer, F8BT, before substrate immersion. F8BT was selected because of electronic considerations; because it is an n-type polymer, it should facilitate, rather than impede, electron transport. Various combination ratios were investigated experimentally, and the 1:1 Cl_4PSi_2:F8BT weight ratio resulting in 10−15 nm IFL films exhibited the highest OPV device performance, and the surface morphology of that blend is depicted in Figure 2c. The surface rms roughness of this blend film (4.05 nm) is approximately the same as that of the plain Cl_4PSi_2 film deposited by the same immersion technique. In the blend film, however, the grains of the underlying ITO are no longer clearly visible under the IFL, signifying more thorough coverage.

Optical Spectroscopy of Cl_4PSi_2. Optical absorption spectra of a film of Cl_4PSi_2 are shown in Figure 3a. Before annealing, one peak is visible at 455 nm. Upon annealing the film on a hot plate in air at 120 °C for 30 min, the main peak is decreased in absorbance and a shoulder peak of nearly equal absorbance appears at λ = 523 nm. The thermal annealing treatment in the presence of water vapor in the air completes the crosslinking of the trimethoxysilane moiety and chemisorbs the molecule onto the hydroxylated substrate. This process ensures a robust IFL adhesion to the underlying ITO and promotes insolubility in all common organic solvents. This trait is demonstrated in Figure 3a by soaking the Cl_4PSi_2-coated substrate in o-dichlorobenzene (ODCB) for 1 min, blowing dry, and observing that the Cl_4PSi_2 absorption curve traces the one taken before soaking. ODCB was selected because it is the solvent typically chosen, and also selected in this work, to deposit the active layer; therefore IFL inertness to this solvent is essential to avoid dissolution during the subsequent device fabrication step. The layer is also completely insoluble if soaked in the solvent blend from which it was deposited, CB:CH_3OH. As a control, the Cl_4PTCDA molecule that was used to synthesize Cl_4PSi_2, but lacks the crosslinking trimethoxysilane groups, was deposited on a substrate and removed with a single CB rinse to confirm that the crosslinking is imperative for insolubility as observed with Cl_4PSi_2.

Figure 3b also illustrates that facile removal of F8BT can be achieved by rinsing in CB:CH_3OH, but two rinses are necessary for its complete removal, likely because the polymer makes relatively good physical contact to the substrate in comparison to a small molecule. When a substrate is immersed into a solution containing a blend of F8BT and Cl_4PSi_2, however, the F8BT is rendered insoluble by the crosslinked Cl_4PSi_2 matrix as illustrated in Figure 3c. This allows incorporation of an n-type polymeric material to aid IFL film formation while maintaining proper energy-level alignment for electron transfer and insolubility for compatibility with the succeeding stages of device fabrication. The absorption of the annealed Cl_4PSi_2:F8BT blend is shown to be slightly different than the pure Cl_4PSi_2 films, lacking the prominent long-wavelength shoulder.

Electrochemical Properties of Cl_4PSi_2. Cyclic voltammetry was used to estimate the LUMO energy of a Cl_4PSi_2 film on ITO. This cyclic voltammogram is displayed in Figure 4 and exhibits a quasi-reversible reduction wave having onset of reduction at -0.2 V vs. SCE and $E_{1/2}$ = -0.41 V. The potential corresponding to the onset of reduction is converted to a LUMO energy of 4.5 eV as described in the Experimental Section. Since common OPV active layer acceptors such as fullerenes typically have LUMO energies of 3.7−4.0, a E_{LUMO} of 4.5 eV designates Cl_4PSi_2 as an energetically well-suited material for accepting electrons in an inverted OPV device architecture.

The HOMO energy of Cl_4PSi_2 was estimated to be ∼7.0 eV from the LUMO energy as derived from electrochemical E_{LUMO} measurements (4.5 eV), the optical band gap as determined from optical spectroscopy (2.2 eV), and an approximation of the exciton binding energy of ∼300 meV. The energy level diagram (inset of Figure 4) illustrates that no energy barrier is expected for electron transfer to Cl_4PSi_2 from PCBM. Additionally, the HOMO energy appears to be sufficiently far from vacuum to efficiently block misdirected holes from the donor polymer HOMO, thereby enhancing diode behavior of the device by

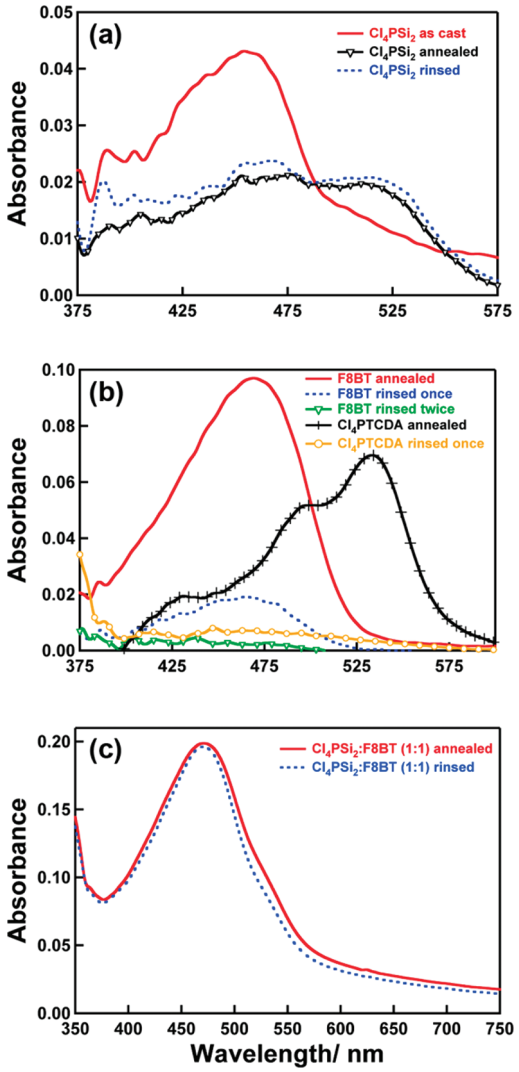

Figure 3. Optical absorption spectra of films: (a) Cl_4PSi_2 before and after annealing, demonstrates insolubility in ODCB after crosslinking. (b) F8BT film alone is completely removed with two rinses in CB:CH_3OH; Cl_4PSi_2 precursor, Cl_4PTCDA, is removed by one rinse in CB. (c) Cl_4PSi_2:F8BT films are insoluble in CB:CH_3OH.

directing opposite polarity charges in the desired opposite directions. The importance of proper IFL energy level alignment in OPVs has been highlighted before using p-type materials,[16,17,25] and the same arguments for the importance of efficient charge transfer, good charge transport through the layer, and effective blocking of undesired charges apply to this IFL. Cl_4PSi_2 appears to possess ideal frontier orbital energies to successfully function as an IFL in inverted OPV devices. Although the F8BT energetics complicate the picture somewhat when this polymer is blended with the Cl_4PSi_2, there is evidently a continuous Cl_4PSi_2 pathway available for electron transfer, because it will be shown below that a Cl_4PSi_2:F8BT blend comprises the IFL yielding the highest device efficiencies in this work.

Inverted OPV devices were fabricated with the common active layer materials P3HT and PCBM and employed a thin ~10 nm film of pure Cl_4PSi_2 (without F8BT) as the n-type IFL. The Cl_4PSi_2 adds a significant amount of series resistance (R_s) to the devices. Therefore a small percentage of a cationic silane was mixed into the layer to reduce the R_s and improve the fill factor

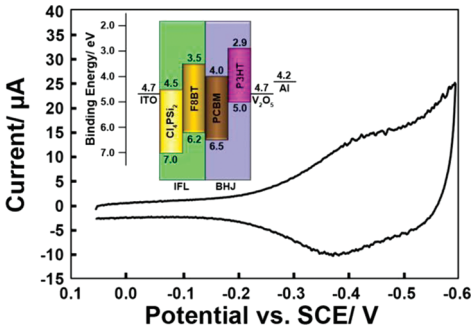

Figure 4. Cyclic voltammogram of a Cl_4PSi_2 film on an ITO working electrode in acetonitrile with 0.1 M $Bu_4N^+PF_6^-$ as the electrolyte. The scan rate was 100 mV/s. Inset: Energy level diagram showing Cl_4PSi_2 insertion into inverted OPV devices as an n-type IFL. ITO, Al, and V_2O_5[54] work functions taken from literature; all organic energy levels determined experimentally from cyclic voltammetry and optical band gap measurements and assume a 0.3 eV exciton binding energy.

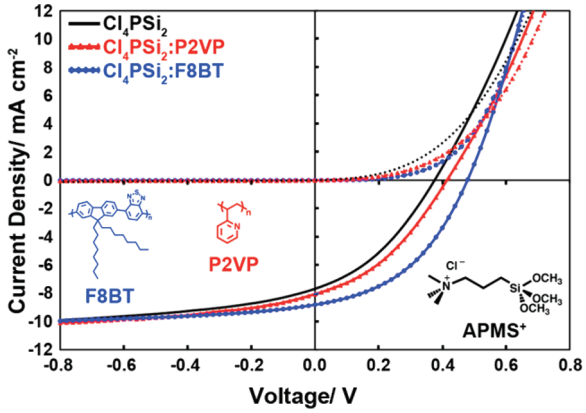

Figure 5. Light (solid lines) and dark (dotted lines) $J-V$ plots of solar cells having various IFLs shown (polymer structures shown as insets), all incorporating 5 wt % APMS$^+$ (structure given in bottom right inset) and having the inverted device architecture ITO/***IFL***/P3HT:PCBM/V_2O_5/Al. All devices were light soaked for 3 min prior to recording the $J-V$ plots.

(*FF*) and overall device performance.[55] The *N*-trimethoxysilylpropyl-*N*,*N*,*N*-trimethylammonium chloride (APMS$^+$) incorporates into the crosslinked Cl_4PSi_2 structure through the same trimethoxysilane moieties used by the PDI to crosslink, and at the low concentrations in which it is added to the Cl_4PSi_2, it does not hamper charge transport. A 0−10% by weight range of APMS$^+$ addition to the Cl_4PSi_2 was investigated, and the 2−5% range increases the *FF* and, in turn, the device performance.

$J-V$ analysis of full devices indicates that the observed V_{oc} for the inverted devices is lower than expected based on the donor HOMO−acceptor LUMO energy gap and on conventional control devices.

There could be various reasons for this, such as the source of P3HT used in this study varying from that of most literature reports, pinholes in the IFL leading to greater charge leakage, or unoptimized vertical alignment of the BHJ morphology for inverted architecture devices. Therefore, in an effort to restore the V_{oc} to a value closer to ~0.5 V, a polymer was blended with the Cl_4PSi_2. First, insulating poly(2-vinylpyridine) (P2VP) was added in a 1:1 wt ratio with Cl_4PSi_2 having 5 wt % of APMS$^+$ also

Table 1. Response Parameters after Light Soaking for Solar Cells Having Inverted Device Architecture

IFL[a]	V_{oc} (V)	J_{sc} (mA/cm^2)	*FF* (%)	η_P (%)
Cl_4PSi_2	0.38	7.69	35.9	1.0
Cl_4PSi_2:P2VP (1:1)	0.41	8.06	36.9	1.2
Cl_4PSi_2:F8BT (1:1)	0.48	8.82	42.9	1.8

[a] IFL indicated has 5 wt % $APMS^+$ incorporated.

present. This addition yielded minimal enhancement in device performance over the plain Cl_4PSi_2 IFL. Next, n-type polymer F8BT was blended with the Cl_4PSi_2 and 5 wt % $APMS^+$. This polymer was shown above (Figure 3c) to exhibit insolubility in ODCB and persist in the IFL when spin-cast with the cross-linking perylene. When F8BT was mixed in solution, 1:1 by wt % with the Cl_4PSi_2 that also had 5 wt % of the $APMS^+$ present, *J*−*V* plots of devices having this IFL exhibited the best inverted device performance in this study. The results are shown in Figure 5 and Table 1. The V_{oc} was successfully increased by adding in the F8BT, about to the expected value for this system, and all device metrics were superior for the Cl_4PSi_2:F8BT IFL blend compared to the Cl_4PSi_2 alone. As a control, devices with just F8BT as the IFL were also fabricated, but these devices largely failed (η_P < 0.1%), likely because there is no silane present to insolubilize the polymer, and the film was mostly dissolved upon active layer deposition from ODCB. Also, the small amount of current generated in these devices flowed in the direction expected for a conventional device. This direction of charge carrier travel is also observed for devices fabricated without any IFL on the ITO, despite using a V_2O_5/Al electrode, likely because the ITO and V_2O_5 have similar work functions, and only a very weak electric field across the device is formed. The Cl_4PSi_2 is apparently imperative to form a selective contact to direct charges in the desired direction. An additional control device omitted the PCBM acceptor to test whether either IFL component could act as an acceptor species and generate photocurrent in an effective bilayer architecture with P3HT, but J_{sc} values for these devices were <0.3 mA/cm^2, proving this contribution to be minimal.

Interestingly, it is necessary to light soak the devices under investigation for ∼3 min to achieve the results shown in Figure 5. Omitting this step results in devices exhibiting very low *FF* and reduced J_{sc}. This phenomenon has been observed before in inverted OPV devices that use, for example, ZnO to modify the ITO.[56] In that case, the specific energy of light required to induce a beneficial change in the *J*−*V* plot must be greater than the band gap of ZnO (∼3.2 eV) and is thought to work by filling any interfacial trap states and lowering the contact resistance. For devices in this work, it appears that light having λ = 400−600 nm, approximately where Cl_4PSi_2 absorbs light, is responsible for inducing the beneficial effect on device performance. A 600 nm long pass filter on top of the device prevents the light soaking procedure from having any effect on device performance, even after an extended light soaking time of 10 min, but the effects are clearly observed via light soaking through a 400 nm long pass filter. Light soaking through a notch filter that transmits light of only λ = 320−390 nm also did not have any effect on device performance. Figure 6 depicts the representative change in *J*−*V* characteristics of a device undergoing light soaking in white light before testing. The *FF* and J_{sc} are both significantly increased from 21.3% and 5.72 mA/cm^2 to 33.1% to 7.37 mA/cm^2, respectively, while the V_{oc} drops only slightly from 0.42 to 0.40 V, resulting

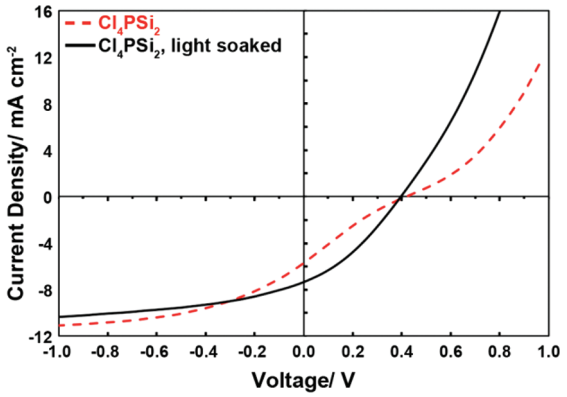

Figure 6. *J*−*V* plots of a solar cell having inverted device architecture ITO/Cl_4PSi_2/P3HT:PCBM/V_2O_5/Al, with Cl_4PSi_2 incorporating 5 wt % $APMS^+$, analyzed before and after light soaking for 3 min.

in a near doubling of η_P from 0.49 to 0.95% after light soaking. The plot reverts slowly over many days to its original state after storing the device in the dark.

4. CONCLUSIONS

A new PDI-based molecule, Cl_4PSi_2, has been synthesized and utilized as an n-type interfacial layer material both by itself and as part of a blended system with polymer F8BT in inverted OPV devices. These IFL films are deposited from solution by an immersion technique and crosslinked via alkoxysilane moieties to induce insolubility across a wide range of solvents, making this IFL amenable to inexpensive, multi-step, solution-processed device fabrication. Topographically smooth films are achieved, and energy levels as measured by CV and optical absorption are aligned well with common OPV active layer materials to transport electrons and block holes. A charged silane molecule is incorporated into the system to reduce the film R_s and enhance device performance. The novel IFL incorporation is demonstrated to be an effective approach to direct charge carriers in the proper direction for inverted OPV function. Also, light soaking prior to device analysis by *J*−*V* plots is shown to be an essential step in characterizing these inverted solar cells, as has been shown before for inverted devices using inorganic IFLs such as ZnO.

AUTHOR INFORMATION

Corresponding Author

*E-mail: ahains@mldevices.com (A.W.H.); brian.gregg@nrel.gov (B.A.G.).

ACKNOWLEDGMENT

We thank Dr. B. To for assistance with AFM measurements and Dr. R. Cormier for helpful discussions. This work was funded by the U. S. Department of Energy, Office of Science, Basic Energy Science, Division of Chemical Sciences, Geosciences, and Biosciences, under Contract DE-AC36-08GO28308 to NREL.

REFERENCES

(1) Hains, A. W.; Liang, Z.; Woodhouse, M. A.; Gregg, B. A. *Chem. Rev.* **2010**, *110*, 6689–6735.
(2) Facchetti, A. *Chem. Mater.* **2011**, *23*, 733–758.

(3) Walker, B.; Kim, C.; Nguyen, T.-Q. *Chem. Mater.* **2011**, *23*, 470–482.
(4) Clarke, T. M.; Durrant, J. R. *Chem. Rev.* **2010**, *110*, 6736–6767.
(5) Deibel, C.; Dyakonov, V. *Rep. Prog. Phys.* **2010**, *73*, 096401.
(6) Li, C.; Liu, M.; Pschirer, N. G.; Baumgarten, M.; Müllen, K. *Chem. Rev.* **2010**, *110*, 6817–6855.
(7) Liang, Y.; Yu, L. *Acc. Chem. Res.* **2010**, *43*, 1227–1236.
(8) Armstrong, N. R.; Wang, W.; Alloway, D. M.; Placencia, D.; Ratcliff, E.; Brumbach, M. *Macromol. Rapid Commun.* **2009**, *30*, 717–731.
(9) Dennler, G.; Scharber, M. C.; Brabec, C. J. *Adv. Mater.* **2009**, *21*, 1–16.
(10) Kippelen, B.; Brédas, J.-L. *Energy Environ. Sci.* **2009**, *2*, 251–261.
(11) Chen, H.-Y.; Hou, J.; Zhang, S.; Liang, Y.; Yang, G.; Yang, Y.; Yu, L.; Wu, Y.; Li, G. *Nat. Photonics* **2009**, *3*, 649–653.
(12) Green, M. A.; Emery, K.; Hishikawa, Y.; Warta, W. *Prog. Photovolt: Res. Appl.* **2010**, *19*, 84–92.
(13) Chen, L.-M.; Xu, Z.; Hong, Z.; Yang, Y. *J. Mater. Chem.* **2010**, *20*, 2575–2598.
(14) Po, R.; Carbonera, C.; Bernardi, A.; Camaioni, N. *Energy Environ. Sci.* **2011**, *4*, 285–310.
(15) Ma, H.; Yip, H.-L.; Huang, F.; Jen, A. K.-Y. *Adv. Funct. Mater.* **2010**, *20*, 1371–1388.
(16) Hains, A. W.; Liu, J.; Martinson, A. B. F.; Irwin, M. D.; Marks, T. J. *Adv. Funct. Mater.* **2010**, *20*, 595–606.
(17) Hains, A. W.; Ramanan, C.; Irwin, M. D.; Liu, J.; Wasielewski, M. R.; Marks, T. J. *ACS Appl. Mater. Interfaces* **2010**, *2*, 175–185.
(18) Reese, M. O.; Morfa, A. J.; White, M. S.; Kopidakis, N.; Shaheen, S. E.; Rumbles, G.; Ginley, D. S. *Sol. Energy Mater. Sol. Cells* **2008**, *82*, 746–752.
(19) Reese, M. O.; White, M. S.; Rumbles, G.; Ginley, D. S.; Shaheen, S. E. *Appl. Phys. Lett.* **2008**, *92*, 053307.
(20) Nanditha, D. M.; Dissanayake, M.; Hatton, R. A.; Curry, R. J.; Silva, S. R. P. *Appl. Phys. Lett.* **2007**, *90*, 113505.
(21) Nelson, J.; Kirkpatrick, J.; Ravirajan, P. *Phys. Rev. B: Condens. Matter* **2004**, *69*, 035337.
(22) Armstrong, N. R.; Veneman, P. A.; Ratcliff, E.; Placencia, D.; Brumbach, M. *Acc. Chem. Res.* **2009**, *42*, 1748–1757.
(23) Stübinger, T.; Brütting, W. *J. Appl. Phys.* **2001**, *90*, 3632–3641.
(24) Kim, J. Y.; Kim, S. H.; Lee, H.-H.; Lee, K.; Ma, W.; Gong, X.; Heeger, A. J. *Adv. Mater.* **2006**, *18*, 572–576.
(25) Hains, A. W.; Marks, T. J. *Appl. Phys. Lett.* **2008**, *92*, 023504.
(26) Irwin, M. D.; Buchholz, D. B.; Hains, A. W.; Chang, R. P. H.; Marks, T. J. *Proc. Natl. Acad. Sci. U.S.A.* **2008**, *105*, 2783–2787.
(27) Kim, D. Y.; Subbiah, J.; Sarasqueta, G.; So, F.; Ding, H.; Irfan; Gao, Y. *Appl. Phys. Lett.* **2009**, *95*, 093304.
(28) Subbiah, J.; Kim, D. Y.; Hartel, M.; So, F. *Appl. Phys. Lett.* **2010**, *96*, 063303.
(29) Li, N.; Lassiter, B. E.; Lunt, R. R.; Wei, G.; Forrest, S. R. *Appl. Phys. Lett.* **2009**, *94*, 023307.
(30) Steirer, K. X.; Chesin, J. P.; Widjonarko, N. E.; Berry, J. J.; Miedaner, A.; Ginley, D. S.; Olson, D. C. *Org. Electron.* **2010**, *11*, 1414–1418.
(31) Ni, J.; Yan, H.; Wang, A.; Yang, Y.; Stern, S. L.; Metz, A. W.; Jin, S.; Wang, L.; Marks, T. J.; Ireland, J. R.; Kannewurf, C. R. *JACS* **2005**, *127*, 5613–5624.
(32) de Jong, M. P.; van IJzendoorn, L. J.; de Voigt, M. J. A. *Appl. Phys. Lett.* **2000**, *77*, 2255–2257.
(33) Wong, K. W.; Yip, H. L.; Luo, Y.; Wong, K. Y.; Lau, W. M.; Low, K. H.; Chow, H. F.; Gao, Z. Q.; Yeung, W. L.; Chang, C. C. *Appl. Phys. Lett.* **2002**, *80*, 2788–2790.
(34) Hau, S. K.; Yip, H.-L.; Baek, N. S.; Zou, J.; O'Malley, K.; Jen, A. K.-Y. *Appl. Phys. Lett.* **2008**, *92*, 253301.
(35) Hau, S. K.; Cheng, Y.-J.; Yip, H.-L.; Zhang, Y.; Ma, H.; Jen, A. K.-Y. *ACS Appl. Mater. Interfaces* **2010**, *2*, 1892–1902.
(36) Motiei, L.; Yao, Y.; Choudhury, J.; Yan, H.; Marks, T. J.; van der Boom, M. E.; Facchetti, A. *JACS* **2010**, *132*, 12528–12530.
(37) Norrman, K.; Madsen, M. V.; Gevorgyan, S. A.; Krebs, F. C. *JACS* **2010**, *132*, 16883–16892.
(38) Krebs, F. C. *Sol. Energy Mater. Sol. Cells* **2008**, *92*, 715–726.
(39) Kim, J. B.; Kim, C. S.; Kim, Y. S.; Loo, Y.-L. *Appl. Phys. Lett.* **2009**, *95*, 183301.
(40) Xu, Z.; Chen, L.-M.; Yang, G.; Huang, C.-H.; Hou, J.; Wu, Y.; Li, G.; Hsu, C.-S.; Yang, Y. *Adv. Funct. Mater.* **2009**, *19*, 1227–1234.
(41) Orimo, A.; Masuda, K.; Honda, S.; Benten, H.; Ito, S.; Ohkita, H.; Tsuji, H. *Appl. Phys. Lett.* **2010**, *96*, 043305.
(42) Chen, L.-M.; Hong, Z.; Li, G.; Yang, Y. *Adv. Mater.* **2009**, *21*, 1434–1449.
(43) Campoy-Quiles, M.; Ferenczi, T.; Agostinelli, T.; Etchegoin, P. G.; Kim, Y. S.; Anthopoulos, T. D.; Stavrinou, P. N.; Bradley, D. D. C.; Nelson, J. *Nat. Mater.* **2008**, *7*, 158–164.
(44) Waldauf, C.; Morana, M.; Denk, P.; Schilinsky, P.; Coakley, K.; Choulis, S. A.; Brabec, C. J. *Appl. Phys. Lett.* **2006**, *89*, 233517.
(45) Park, M.-H.; Li, J.-H.; Kumar, A.; Li, G.; Yang, Y. *Adv. Funct. Mater.* **2009**, *19*, 1241–1246.
(46) Wang, J.-C.; Weng, W.-T.; Tsai, M.-Y.; Lee, M.-K.; Horng, S.-F.; Perng, T.-P.; Kei, C.-C.; Yu, C.-C.; Meng, H.-F. *J. Mater. Chem.* **2010**, *20*, 862–866.
(47) Kyaw, A. K. K.; Sun, X. W.; Jiang, C. Y.; Lo, G. Q.; Zhao, D. W.; Kwong, D. L. *Appl. Phys. Lett.* **2008**, *93*, 221107.
(48) White, M. S.; Shaheen, S. E.; Kopidakis, N.; Ginley, D. S. *Appl. Phys. Lett.* **2006**, *89*, 143517.
(49) Shirakawa, T.; Umeda, T.; Hashimoto, Y.; Fujii, A.; Yoshino, K. *J. Phys. D: Appl. Phys.* **2004**, *37*, 847–850.
(50) Li, G.; Chu, C.-W.; Shrotriya, V.; Huang, J.; Yang, Y. *Appl. Phys. Lett.* **2006**, *88*, 253503.
(51) Liao, H.-H.; Chen, L.-M.; Xu, Z.; Li, G.; Yang, Y. *Appl. Phys. Lett.* **2008**, *92*, 173303.
(52) Bard, A. J.; Faulkner, L. R., *Electrochemical Methods: Fundamentals and Applications*, 2nd ed.; John Wiley & Sons: New York, 2001.
(53) Cardona, C. M.; Li, W.; Kaifer, A. E.; Stockdale, D.; Bazan, G. C. *Adv. Mater.* **2011** in press.
(54) Shrotriya, V.; Li, G.; Chu, C.-W.; Yang, Y. *Appl. Phys. Lett.* **2006**, *88*, 073508.
(55) Reilly, T. H.; Hains, A. W.; Chen, H.-Y.; Gregg, B. A. *Adv. Energy Mater.* **2011**, submitted.
(56) Lloyd, M. T.; Peters, C. H.; Garcia, A.; Kauvar, I. V.; Berry, J. J.; Reese, M. O.; McGehee, M. D.; Ginley, D. S.; Olson, D. C. *Sol. Energy Mater. Sol. Cells* **2011**, *95*, 1382–1388.